analytical chemistry

Article

pubs.acs.org/ac

Label-Free Detection of Cardiac Troponin-I Using Carbon Nanofiber Based Nanoelectrode Arrays

Adaikkappan Periyakaruppan, Ram P. Gandhiraman, M. Meyyappan, and Jessica E. Koehne*

Center for Nanotechnology, NASA Ames Research Center, Moffett Field, California 94035, United States

ABSTRACT: A label-free biosensor is presented using carbon nanofiber (CNF) nanoelectrode arrays for the detection of cardiac troponin-I in the early diagnosis of myocardial infarction. Immobilization of anti-cTnI Ab on CNFs and the detection of human-cTnI were examined using electrochemical impedance spectroscopy and cyclic voltammetry techniques. Each step of the modification process was monitored, and the results show changes in electrical capacitance or resistance to charge transfer due to the specificity of corresponding adsorption of Ab−Ag interaction. The immunosensor demonstrates a good selectivity and high sensitivity against human-cTnI analytes and is capable of detecting cTnI at concentrations as low as ~0.2 ng/mL, which is 25 times lower than that possible by conventional methods. Analysis of the electrode at various stages using atomic force microscopy and X-ray reflectivity provides information on the surface roughness and orientation of the antibody.

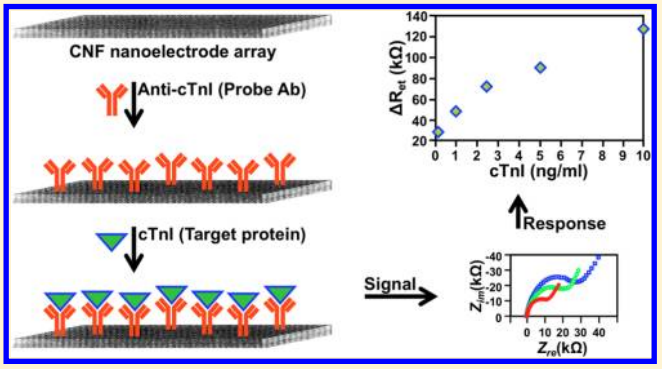

Acute myocardial infarction (AMI) is the cause of one of the highest mortality rates in the United States and responsible for one-third of deaths in the world. This underscores early diagnosis as critical for the treatment of AMI. Cardiac biomarkers in blood sample provide an effective way to diagnose the illness,[1] and elevated levels of these markers are an independent predictor of morbidity and mortality. Biomarkers for the detection of cardiac infarction include creatine kinase MB (CK-MB), myoglobin, cardiac troponins (cTn), and myeloperoxidase (MPO).[2] Among them, cardiac troponin-I has been recognized as a principal biomarker[3] due to its excellent specificity and great sensitivity for acute myocardial cell damage.[4−6] The levels of cardiac troponin-I in healthy humans are normally lower than 0.4 ng/mL, and levels greater than 2.0 ng/mL indicate an increased risk for future serious heart events. This emphasizes the need for developing diagnostic tools which are sensitive, cost-effective, and utilize existing large-scale manufacturing techniques.

The diagnostic techniques for AMI have included conventional enzyme-linked immunosorbent assay (ELISA)[7] and radioimmunoassay (RIA).[8,9] The issues with these approaches include sensitivity, multistep processing of samples, long diagnostics times, and the overall cost. In this regard, biosensors for protein detection have become common and cost-effective, showing high sensitivity and multiplexing capability.[10] A recent review of biosensors for the detection of cardiac biomarkers can be found in ref 11 which discusses various markers, detection techniques, and sensor platforms. Among the detection techniques, electrochemical approaches such as cyclic voltammetry (CV) and electrochemical impedance spectroscopy (EIS) have been widely used for their potential for the real-time monitoring of biomolecule interaction such as protein, nucleic acid, etc. in contact with the sensor electrode surface.[12−15] EIS has been shown to have great potential for label-free detection, simplifying the molecular recognition process and enhancing the sensitivity.[15]

In recent years, carbon-based nanostructures, such as carbon nanotubes (CNTs), nanofibers, and graphene as well as various inorganic nanowires have shown great potential for developing biosensors with improved sensitivity.[16−18] Platforms using these nanomaterials have been used for the detection of cardiac biomarkers with superior sensitivity.[19−21] Though detection limits of pico-/femtogram levels have been reported, current limitations include long duration of assay processing, expensive tools, and use of highly toxic substances. Hence, new approaches with high sensitivity and specificity are needed for the detection of cTnI without the need for high-cost equipment. Compared to single- and multiwalled CNTs, carbon nanofibers (CNFs) grown by plasma-enhanced chemical vapor deposition (PECVD) are individual, free-standing, and vertical nanostructures ideal for construction of nanoelectrode arrays (NEA). Wafer-scale fabrication of NEAs, attaching various DNA, antibody, and aptamer probes to the CNF electrodes, and subsequent sensing demonstration using electrochemical impedance spectroscopy have been reported.[22−25]

In the present study, we have demonstrated a simple, label-free, point-of-care immunosensor signal amplification method to detect myocardial symptomatic biomarker troponin-I using

Received: September 26, 2012
Accepted: February 5, 2013
Published: February 5, 2013

   dx.doi.org/10.1021/ac302801z | *Anal. Chem.* 2013, 85, 3858−3863

vertically aligned carbon nanofiber (VACNF)-based nanoelectrode arrays. Two key challenges in biosensing, that are dependent on the surface chemistry and topography of the sensing chip, are nonspecific binding and accessibility of active sites of the immobilized ligand toward analyte.[26,27] Reducing the nonspecific binding is critical in label-free biosensing techniques as the binding of any nonanalyte constituents would give rise to false positive errors. If the immobilized ligand (antitroponin) is flat or upside down or if there is steric hindrance, the active sites would no longer be available for analyte binding and would result in decreased sensitivity.[28] Hence, both the surface roughness and the orientation of the antibody are important factors for highly sensitive label-free detection. Therefore, X-ray reflectivity (XRR) and atomic force microscopy (AFM) techniques are used here to study the surface roughness and orientation of the capture antibody. Cyclic voltammetry and electrochemical impedance spectroscopy measurements show a low detection limit of ~0.2 ng/mL with linearity, high sensitivity, and good specificity.

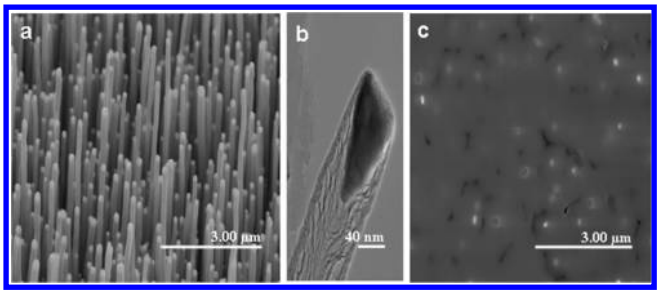

Figure 1. (a) SEM image of an as-grown vertically aligned carbon nanofiber array: magnification = 15 000×, HV = 10.0 kV. (b) TEM image of a stacked cone morphology of carbon nanofibers. This represents the top portion of the fiber as the bottom portion is attached to the silicon wafer. The open-ended tip is characteristic of nanofibers and is important for sensing applications which require functionalization of the carbon surface: magnification = 100 000×, HV = 300 kV. (c) The nanoelectrode array after CMP showing tips of the VACNFs: magnification = 18 000×, HV = 15.0 kV.

EXPERIMENTAL SECTION

Reagents. Human cardiac troponin-I (cTnI) as a highly pure antigen protein, mouse anticardiac troponin-I (anti-cTnI) monoclonal (1E7) as an antibody, and an equine cardiac myoglobin (≥95%) as a control antigen protein, *N*-hydroxysulfosuccinimide sodium salt (sulfo-NHS 98%), and 1-ethyl-3-(3-dimethylamino propyl)-carbodiimide (EDC 99%) as a reactive cross-linkers, potassium hexacyanoferrate(II) trihydrate ($K_4Fe(CN)_6$), and all other reagents used were of analytical grade and purchased from Sigma-Aldrich (St. Louis, MO). All solutions were prepared with deionized water.

Apparatus. Cyclic voltammetry and electrochemical impedance spectroscopy measurements were performed using a CH Instruments electrochemical workstation equipped with frequency response analyzer (660D), interfaced with a personal computer, and controlled by chi 660d software (CH Instruments Inc., Austin, TX). The electrochemical experiments were carried out using the CNF-based NEA as working electrode, a platinum wire auxiliary as counter electrode, and a saturated calomel electrode (SCE) as reference electrode, respectively. The size of the working electrode was defined by a 3 mm O-ring sealed in a custom-built liquid cell, as previously described.[22] Electrical contact to the working electrode was made using a spring-loaded pin to contact an underlying Cr film lead that extends out of the liquid cell. All reported potentials in this work are referenced to SCE. All measurements were carried out under ambient temperature (25 ± 1 °C). The structural characterization of VACNFs was done by scanning electron microscopy (SEM) (S4800, Hitachi, Pleasanton, CA) and transmission electron microscopy (TEM) (H9500, Hitachi, CA). Detection of human-cTnI analytes binding toward the CNF electrode was done by a Nanoscope multimode atomic force microscope (AFM) tool (Digital Instruments, Santa Barbara, CA), and images were acquired in contact mode using an ORC8 silicon nitride cantilever with a 0.1 N/m spring constant (Veeco, Santa Barbara, CA).

Electrode and Biosensor Fabrication. Individual, free-standing, vertically aligned carbon nanofibers as a nanoelectrode array were grown by PECVD on a silicon wafer. Figure 1 shows a representative image of a VACNF array. Though individual CNF nanoelectrodes can be precisely positioned using lithographic patterning, the present demonstration utilizes a randomly grown CNF array wherein the average distance between adjacent electrodes is about 1 μm. Growth of the VACNF array and fabrication details have been reported previously,[22−25] and only a brief account is given here. A 200 nm chromium layer was sputtered onto a silicon wafer with 500 nm thick thermal oxide, followed by a thin layer of nickel (30 nm) sputtered as catalyst. A dc-biased PECVD system (Aixtron, Cambridge, U.K.) was used to grow VACNFs with acetylene as feedstock (125 sccm) and ammonia as diluent (444 sccm) at 6.3 mbar, 700 °C, and 180 W of power. The VACNFs are typically 100 nm in diameter at the bottom and 80 nm at the tip and are ~3 μm tall for a growth time of 15 min. Individual VACNFs were electrically isolated from each other by depositing SiO_2 as a dielectric using chemical vapor deposition with tetraethoxysilane as precursor. The oxide completely encapsulates each fiber, and a subsequent chemical mechanical polishing (CMP) step provides a smooth SiO_2 top surface with only tips of the VACNFs protruding above the surface. This type of electrode surface was previously found to be necessary to observe changes in charge-transfer resistance using electrochemical impedance spectroscopy.[25] The CMP process consists of two steps: stock removal and final polish. A 0.5 μm alumina (pH 4) at 10 mL/min, 60 rpm platen, 15 rpm carrier, and 15 psig down force was used to remove bulk material at ~150 nm/min. A 0.1 μm alumina (pH 4) at 10 mL/min, 60 rpm platen, 15 rpm carrier, and 25 psig down force was used for the final polish at ~20 nm/min. The wafers were cleaned in a mixture of water, hydrogen peroxide, and ammonium hydroxide (80:2:1) and spin-dried. As-grown VACNFs and the nanoelectrode array after CMP are shown in Figure 1.

Electrochemical Measurements. The CNF electrodes prepared as above were characterized electrochemically prior to their use in troponin detection. They were pretreated by soaking in 1.0 M HNO_3 for 15−30 min and washed with sterile water prior to electrochemical characterization for several reasons: removal of damage, if any, to the VACNF tips during various fabrication steps, improving electrode kinetics by decreasing the peak-to-peak separation for standard redox species, and introducing −COOH groups for subsequent covalent binding of the probe antibody. Electrochemical properties of the bare unmodified VACNFs chips were evaluated through CV and EIS as described previously.[24] In

dx.doi.org/10.1021/ac302801z | *Anal. Chem.* 2013, 85, 3858−3863

brief, the CV data were recorded between −0.4 and 0.8 V versus SCE with a scan rate of 20 mV s^{-1} in a solution of 5 mM $K_4Fe(CN)_6$ in 0.1 M phosphate buffer (pH 7.4) (1:1 mixture). EIS measurements were carried out in a mixture of 5 mM $K_4Fe(CN)_6$ in 0.1 M KCl. The spectra were taken at 0.1 Hz to 100 kHz at open circuit potential versus SCE.

Electrochemical Detection of Cardiac Troponin-I. The VACNF sensor electrode with immobilized target was prepared as described earlier.[23] In brief, 5 μg/mL anti-cTnI antibody was suspended in 50 μL of PBS containing 0.25 mg of sulfo-NHS and 0.5 mg of EDC and incubated at room temperature for 1 h. In this process, the overlaying probes are bound onto the CNF electrode surface by means of the functional groups. The electrodes were stringently washed three times with PBS buffer to eliminate the nonspecific binding conjugates. The modification of probe anti-cTnI bound to the CNF nanoelectrodes was evaluated through CV and EIS measurements.

Similarly, 0.0−0.1 μg/mL human-cTnI in a 50 μL of PBS solution was incubated with probe-immobilized CNF electrodes at room temperature for 1 h. The process carries the immunoreaction between the target human-cTnI and moiety anti-cTnI on the surface electrode. Then, the electrodes were washed vigorously with PBS buffer for 10 min to eliminate the nonspecific sites. The detection of cardiac human-cTnI binding on the CNFs electrodes was accomplished through CV and EIS measurements. The entire target−analyte binding detection was repeated using 0.0−1.0 μg/mL cardiac myoglobin, a nonspecific cardiac targeted protein for control purposes.

AFM Analysis of the Functionalized Electrodes. Tapping mode AFM images were acquired for VACNF-based NEAs to characterize the sensor surface topography of immobilized antigen−antibody binding.[23] The images were taken by dampening the resonant frequency of the cantilever by 20−40% and a scanning rate of 3 μm/s and collected with a resolution of 512 × 512 pixel frame, at scan rates of 1.0 Hz. Images of height and deflection were acquired simultaneously. At each surface, two to three independent regions were used to collect images of 20 μm by 20 μm. The width and height of immobilized antibody and protein were determined using section profiles of the captured AFM images. A total of 30 section profiles were collected for each grain size. The number of features was manually counted in each AFM image and divided by the width of the image in micrometers to determine the density. All immobilized electrochemical immunoassay binding was assayed twice in order to confirm by AFM characterization.

X-ray Reflectivity. The XRR experiments were performed at the Stanford Synchrotron Radiation Light (SSRL) Source on the thin-film diffraction beamline 2-1, equipped with a Huber 2-circle goniometry. X-rays of 1.55 Å were monochromated with a Si(111) double crystal. Reflected X-rays were collimated by a pair of 1 mm slits and detected with a Bicron NaI detector. The thickness and roughness calculations were carried out using GenX software that generates a theoretical reflectivity scan based on the inputs provided.

ELISA-Based Detection of Troponin-I. ELISA procedure for the detection of human-cTnI was performed for comparison as described by Velden et al.,[29] with small modifications. In brief, 50 ng/μL anti-cTnI diluted with PBS was applied in a 96-well plate and incubated at 4 °C for overnight. Then the binding sites were blocked with 5% bovine serum albumin and 0.05% Tween-20 for 1 h, washed with PBST (PBS with 0.05% of Tween-20), and incubated with 0.0−1.0 μg/mL human-cTnI for 2 h at room temperature. Further washing with PBST thrice and incubation with 50 ng/μL polyclonal goat antimouse immunoglobulin for 2 h followed by horseradish peroxidase (HRP) for 1 h at room temperature was done with final wash with PBST thrice. The plates were then incubated with citrate buffer containing 400 μg/mL *o*-phenylenediamine (OPD) and 0.03% (v/v) hydrogen peroxide for 30 min at room temperature and added 2 mmol/L H_2SO_4. The optical density (OD) was read at 450 nm (Thermo Lab System/Multiskan RC plate reader) relative to a blank obtained by adding PBS to the wells, and myoglobin was used as a nonspecific control instead of human-cTnI in the required initial steps.

RESULTS AND DISCUSSION

The size and separation of individual VACNF electrodes in the NEA are key parameters which determine the nanoelectrode performance.[25] SEM images of as-grown VACNFs and the electrode array with VACNFs embedded in silicon dioxide to make the NEAs are shown in Figure 1. The as-grown VACNFs are well-aligned, approximately 3 μm tall, and have diameters ranging from 50 to 100 nm. The TEM image in Figure 1b shows the bamboo-like structure of the carbon nanofiber with the catalyst particle on the top. These particles are removed easily during the CMP process. Figure 1c shows that each nanofiber is completely encapsulated by SiO_2. After SiO_2 encapsulation and CMP, the mean separation distance between individual electrodes is approximately 700 nm, which is ideal to maintain nonoverlapping hemispherical diffusion layers around each VACNF. Steady-state cyclic voltammograms serve as further confirmation of ideal separation of nanofiber electrodes in the array. The NEA chips in this study showed steady-state behavior (data not shown here) in 5 mM $K_4Fe(CN)_6$ in 0.1 M phosphate buffer (pH 7.4) (1:1 mixture).

The sequential modification of the electrodes immobilized with the probe anti-cTnI and target human-cTnI was characterized using steady-state CVs, recorded between −0.3 and +0.8 V versus SCE with a scan rate of 20 mV s^{-1} in a solution of 0.1 M PBS (pH 7.4) containing 1 mM $K_4Fe(CN)_6$. The $Fe(CN)_6$ shows reversible one-electron redox peaks in bare CNF-based NEAs with a peak-to-peak separation (Figure 2i, curve a). The immobilization of anti-cTnI on the CNF electrode decreases the current response of the sensor, due to the substantial blockage on the electrode surface by the probes (Figure 2i, curve b). Subsequently, a significant decrease in current is noticed after target human-cTnI bound onto the capture moiety immobilized nanoelectrode (Figure 2i, curve c), suggesting a change in the electron transfer at the surface. This signifies the successful occurrence of the probe anti-cTnI and target detector human-cTnI interaction on the electrode surface.

Adsorption of antibody and detection of target were also characterized using EIS by monitoring the changes in the electron-transfer resistance of the electrode R_{ct}. EIS is a sensitive technique for analyzing the changes in the properties of the electrode surface. The semicircle diameter in the Nyquist plot corresponds to the electron-transfer resistance (R_{ct}) which controls the electron-transfer kinetics of the redox probe at the electrode interface.[23,24] The Nyquist plot in Figure 2ii presents the R_{ct} responses at different stages of capture Ab and target human-cTnI immobilization on the nanoelectrode array. The bare CNF electrode shows a low interfacial charge-transfer resistance (14.9 kΩ) (curve a in Figure 2ii). The R_{ct} value increases after immobilization of capture moiety anti-cTnI,

dx.doi.org/10.1021/ac302801z | *Anal. Chem.* 2013, 85, 3858−3863

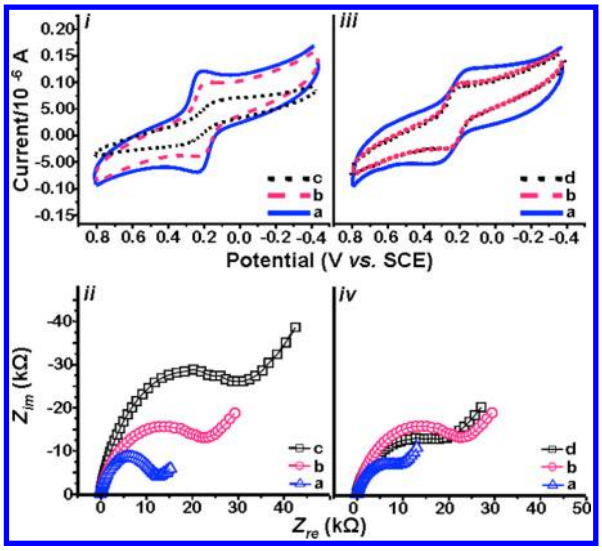

Figure 2. (i and iii) Cyclic voltammograms of the VACNF electrode recorded in PBS containing 5 mM $Fe(CN)_6^{3-}/Fe(CN)_6^{4-}$ and 0.1 M KCl. Scan rate was 20 mV s^{-1}. (ii and iv) Nyquist plots of the electrode recorded in PBS containing 5 mM $Fe(CN)_6^{3-}/Fe(CN)_6^{4-}$ and 0.1 M KCl. The frequency range is from 0.01 Hz to 100 kHz with signal amplitude of 10 mV, and the scan rate was 0.1 V s^{-1}. (i and ii) Specificity of human-cTnI detection. (iii and iv) Nonspecific control protein detection: (a) bare electrode; (b) bare/anti-cTnI electrode; (c) bare/anti-cTnI/human cTnI electrode; (d) bare/anti-cTnI/human myoglobin electrode.

which perturbs the interfacial electron-transfer rate formed on the electrode surface (30.3 kΩ) (Figure 2ii, curve b). The subsequent binding of the target results in a significant increase (by 37%) in the electron-transfer resistance (45.9 kΩ) (Figure 2ii, curve c). These results, along with the CV measurements, confirm the successful immobilization of anti-cTnI and human-cTnI without any amplification process.

To further confirm the cross-reactivity of the immunosensors, the CNF electrode was evaluated under similar set of CV and EIS experiments using equal concentration of myoglobin. Myoglobin is a cardiac-related biomarker used as a control nonspecific target in this experiment. Figure 2iii shows insignificant differences in current after immobilization of nonspecific myoglobin protein to the anti-cTnI electrode, providing evidence for the absence of binding between myoglobin protein and anti-cTnI. Figure 2iv provides similar evidence using EIS with the myoglobin protein incubated with the antibody-immobilized CNF electrode showing no change in the R_{ct} value (Figure 2, curves b and d), which indicates that no interaction occurred between anti-cTnI and myoglobin. These data confirm the selectivity of the immunoassay procedure and provide evidence that there is no adsorption after immobilizing with myoglobin protein.

Surface functionalization, roughness, and topography of the chip play a crucial role in controlling the nonspecific adsorption and in determining the conformation of the adsorbed protein layer.[30] It has been reported that nanoscale surface roughness directly influences the nonspecific binding, with the nonspecific adsorption decreasing with decrease in surface roughness.[26,31] In order to characterize the surface topology of the modified VACNFs, AFM analysis of the electrode was performed under various stages: bare electrode, after adsorption of anti-cTnI, and binding of human-cTnI. Figure 3 presents the topographical images of three-dimensional height plots for the electrode under these conditions. The morphology of the bare electrode shows a smooth surface of the height profile, ∼2 nm as shown in Figure 3, parts a and d, which is consistent with earlier results.[23,32] The surfaces covered by anti-cTnI antibodies and human-cTnI proteins coupled with the antibodies are much rougher than the bare electrode surface. As shown in Figure 3, parts b and e, and parts c and f, the resulting morphologies under these stages show height profiles of ∼17 and ∼52 nm, respectively. The height differences seen here provide additional confirmation besides electrochemical measurements for the probe immobilization and the probe−target binding.

The XRR scan profile is shown in Figure 4. The surface roughness of the polished CNF array measured using X-ray reflectivity is 2 nm. The surface roughness increases upon binding of the antibody, which is in agreement with ref 33 as well as the AFM data above. The thickness values measured using XRR were found to be 16, 17, and 15 nm, respectively, for anti-cTnI antibody with three different concentrations of 0.5, 5.0, and 20.0 μg/mL. Measured thickness of the bound antibody layer is in close agreement with the AFM data of 17 nm for anti-cTnI binding. The physical size of an antibody measured using X-ray crystallography has a length of 14 nm and a width of 7.5 nm.[34,35] The thickness measurement here shows

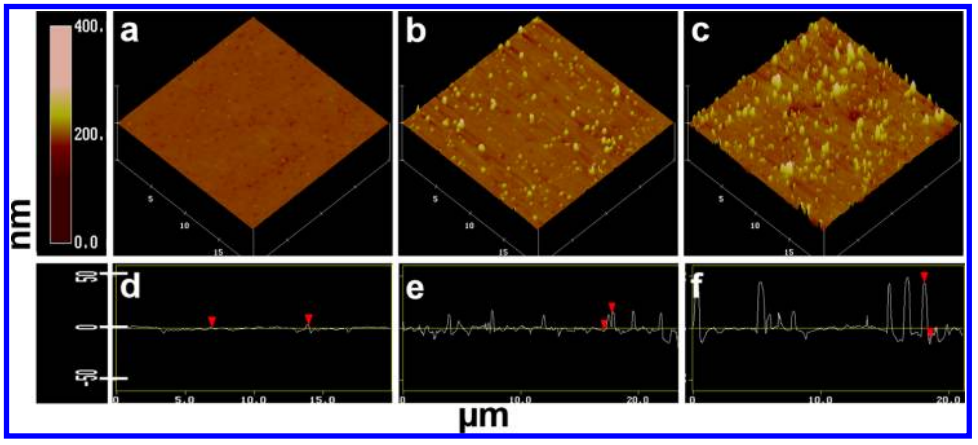

Figure 3. Three-dimensional AFM images of the VACNF electrode: (a−c) surface plot topography and (d−f) measured feature section analysis of vertical height distance topographs: (a and d) bare electrode; (b and e) electrode after immobilization with anti-cTnI; (c and f) after human cTnI binding to the electrode immobilized with anti-cTnI.

dx.doi.org/10.1021/ac302801z | Anal. Chem. 2013, 85, 3858−3863

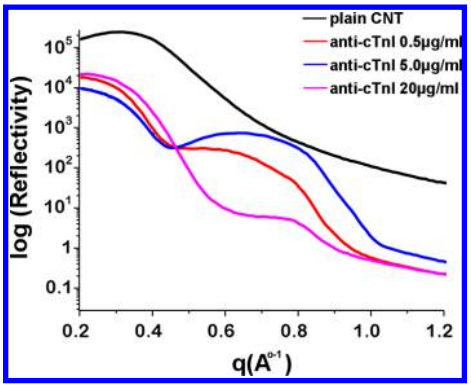

Figure 4. X-ray reflectivity profile of chemical mechanical polished CNF immobilized with varying concentrations of anti-cTnI antibody.

that the antibody is oriented vertically, and hence, the active sites are readily available for analyte binding. The roughness values for the CNF chips immobilized with anti-cTnI antibody are 3.8, 3.3, and 4.5 nm, respectively, for 0.5, 5.0, and 20 μg/mL anti-cTnI concentrations. The observed difference in roughness is probably due to the fact that different concentrations of surface-bound antibody result in different densities of packing. The minor variation in thickness could be attributed to a slight change in the orientation of the antibody, as a result of different densities of packing, that would affect both the thickness and the roughness as observed.

To assess the sensitivity of the detection platform, the effect of different concentrations of human-cTnI and the target-specific anti-cTnI was studied through EIS measurements. The Nyquist plots fitted perfectly by a Randle equivalent circuit model reveal that the R_{ct} is suitable to evaluate concentration-dependent characteristics. Figure 5 shows the impedimetric responses of the sensor electrode for various concentrations of

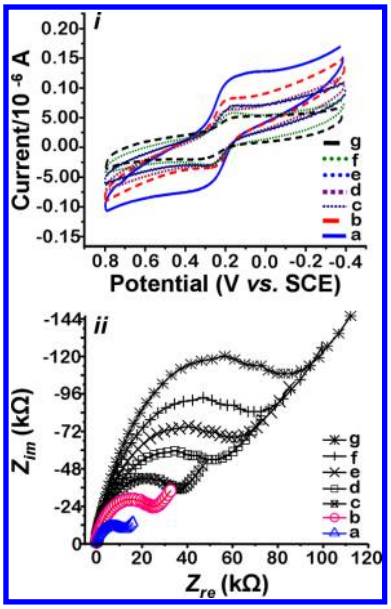

Figure 5. (i) Cyclic voltammograms and (ii) Nyquist plots of a VACNF electrode before and after incubating with different concentrations of human-cTnI in PBS containing 5 mM Fe-$(CN)_6^{3-}$/$Fe(CN)_6^{4-}$ and 0.1 M KCl: (a) bare electrode; (b) bare/anti-cTnI electrode; curves c–g represent 0.25, 0.5, 1.0, 5.0, and 10.0 ng/mL human cTnI antigen binding to the bare electrode after immobilization with anti-cTnI antibody, respectively.

human-cTnI (0.0, 0.25, 0.5, 1.0, 5.0, and 10.0 ng/mL). The diameter of the Nyquist circle notably increases with increasing concentration of human-cTnI. This possibly could be due to the ability of more analytes binding to the immobilized antibodies in higher concentration of target antigens (cTnI), which work as a definite kinetic barrier for the electron-transfer resistance. The limit of detection is 0.2 ng/mL. For comparison, results from a label-based system like the conventional ELISA method show a detection limit of 5 ng/mL (data not shown), which is about 25 times higher than our direct label-free detection method. The long-term stability of the CNF sensor was studied by a series of three immunoassays for the detection of 0.2 and 1.0 ng/mL. The relative standard deviation (RSD) of the measurements was ±3.9% for 0.2 ng/mL human-cTnI and ±2.1% for 1.0 ng/mL human cTnI, respectively, suggesting that the assay is reproducible in the tested conditions.

Specificity of the label-free immunosensing electrode was studied using different concentrations (0.1–100 ng/mL) of human-cTnI (specific) protein and myoglobin (nonspecific) control protein. Figure 6 shows the calibration plots for the

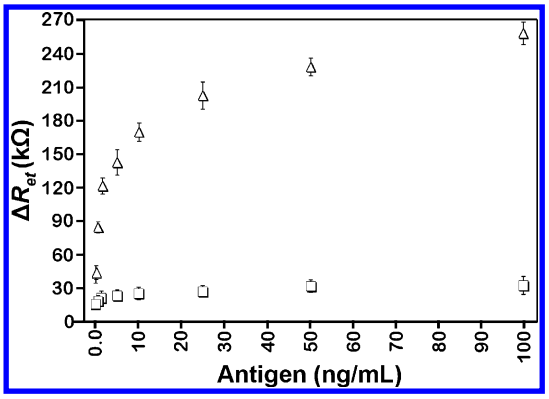

Figure 6. Calibration plots showing ΔR_{ct} for different concentrations of (Δ) human cTnI, a specific target protein analyte, and (□) human myoglobin, an unrelated nonspecific analyte for the VACNFs immunosensor electrode.

equivalent circuit model of the CNF-based NEAs corresponding to the Nyquist plots. Three sets of experiments were conducted for each concentration, and standard deviations are illustrated by the error bars in Figure 6. The sensor shows a linear R_{ct} to concentration relationship in the range of 0.25–1.0 and 5.0–100 ng/mL with correlation coefficients of 0.94528 and 0.89790, respectively. The electron-transfer resistance increases with an increase in the concentration of human cTnI bindings as expected, but no significant changes with increased concentration of control protein myoglobin. This confirms that the observed changes in the electron-transfer resistance with human cTnI are due to specific antigen–antibody interaction without interference from the unrelated protein.

CONCLUSIONS

An inexpensive, easy, and label-free electrochemical impedance spectroscopy based biosensor has been developed for the selective detection of human-cTnI, a cardiac biomarker for the early diagnosis of AMI. The sensor consists of a nanoelectrode array of vertical carbon nanofibers, and the results here show a low detection limit of 0.2 ng/mL cTnI concentration. Data

dx.doi.org/10.1021/ac302801z | Anal. Chem. 2013, 85, 3858–3863

from conventional ELISA technique obtained for comparison shows a detection limit 25 times higher at 5 ng/mL.

AUTHOR INFORMATION

Corresponding Author

*E-mail: jessica.e.koehne@nasa.gov.

Notes

The authors declare no competing financial interest.

ACKNOWLEDGMENTS

A.P. acknowledges Dr. Olufisayo Jejelowo and Dr. Adebayo Oyekan of Texas Southern University and Dr. Govindarajan Ramesh of Norfolk State University for their support. A.P. is a visiting Postdoctoral Fellow from TSU, Houston, supported by a NASA URC contract to TSU (NNX08BA47A). R.P.G. is a visiting research scholar from Dublin City University, Ireland under the Science Foundation Ireland fellowship 10/CE/B1821-STTF 11. The authors acknowledge Dr. Apurva Mehta and Dr. Michael F. Toney from Stanford Synchrotron Radiation Light Source (SSRL), Stanford University for their help in X ray reflectivity measurement.

REFERENCES

(1) McDonnell, B.; Hearty, S.; Leonard, P.; O 'Kennedy, R. *Clin. Biochem.* **2009**, *42*, 549.
(2) Friess, U.; Stark, M. *Anal. Bioanal. Chem.* **2009**, *393*, 1453.
(3) Fredericks, S.; Merton, G.; Lerena, M. J.; Holt, D. W. *Clin. Chem.* **1998**, *44*, 362.
(4) Amodio, G.; Antonelli, G.; Varraso, L.; Ruggieri, V.; Di Serio, F. *Coron. Artery Dis.* **2007**, *18*, 181.
(5) Cummins, B.; Auckland, M. L.; Cummins, P. *Am. Heart J.* **1987**, *113*, 1333.
(6) Mahmarian, J. J. *J. Nucl. Cardiol.* **2007**, *14*, 6.
(7) Wang, J.; Ibanez, A.; Chatrathi, M. P.; Escarpa, A. *Anal. Chem.* **2001**, *73*, 5323.
(8) Apple, F. S.; Falahati, A.; Paulsen, P. R.; Miller, E. A.; Sharkey, S. W. *Clin. Chem.* **1997**, *43*, 2047.
(9) Carraro, P.; Plebani, M.; Varagnolo, M. C.; Zaniotto, M.; Rossetti, M.; Burlina, A. *J. Clin. Lab. Anal.* **1994**, *8*, 70.
(10) Vo-Dinh, T.; Cullum, B. J. *Anal. Chem.* **2000**, *366*, 540.
(11) Quereshi, A.; Gurbuz, Y.; Niazi, J. H. *Sens. Actuators, B* **2012**, *171*, 62.
(12) De Marco, R.; Pejcic, B. *Anal. Chem.* **2000**, *72*, 669.
(13) Lisdat, F.; Schafer, D. *Anal. Bioanal. Chem.* **2008**, *391*, 1555.
(14) Patolsky, F.; Lichtenstein, A.; Willner, I. *J. Am. Chem. Soc.* **2001**, *123*, 5194.
(15) Bogomolova, A.; Komarova, E.; Reber, K.; Gerasimov, T.; Yavuz, O.; Bhatt, S.; Aldissi, M. *Anal. Chem.* **2009**, *81*, 3944.
(16) Li, J. *Biosensors in Carbon Nanotubes: Science and Applications*; Meyyappan, M., Ed.; CRC Press: Boca Raton, FL, 2004.
(17) Alwarappan, S.; Erdem, A.; Liu, C.; Li, C.-T. *J. Phys. Chem. C* **2009**, *113*, 8853.
(18) Meyyappan, M.; Sukara, M. K. *Inorganic Nanowires: Applications, Properties and Characterization*; CRC Press: Boca Raton, FL, 2010; Chapter 14.
(19) Chua, J. H.; Chee, R.-E.; Agarwal, A.; Wong, S. M.; Zhang, G.-J. *Anal. Chem.* **2009**, *81*, 6266.
(20) Jagadeesan, K. K.; Kumar, S.; Sumana, G. *Electrochem. Commun.* **2012**, *20*, 71.
(21) Lee, I.; Luo, X.; Huang, J.; Cui, X. T.; Yun, M. H. *Biosensors* **2012**, *2*, 205.
(22) Koehne, J. E.; Chen, H.; Li, J.; Cassell, A. M.; Ye, Q.; Ng, H. T.; Han, J.; Meyyappan, M. *Nanotechnology* **2003**, *14*, 1239.
(23) Periyakaruppan, A.; Arumugam, P. U.; Meyyappan, M.; Koehne, J. E. *Biosens. Bioelectron.* **2011**, *28*, 428.
(24) Arumugam, P. U.; Chen, H.; Siddiqui, S.; Weinrich, J, A.; Jejelowo, A.; Li, J.; Meyyappan, M. *Biosens. Bioelectron.* **2009**, *24*, 2818.
(25) Siddiqui, S.; Arumugam, P. U.; Chen, H.; Li, J.; Meyyappan, M. *ACS Nano* **2010**, *4*, 955.
(26) Choi, S.; Chae, J. *J. Micromech. Microeng.* **2010**, *20*, 5015.
(27) Jonkheijm, P.; Weinrich, D.; Schroder, H.; Niemeyer, C. M.; Waldmann, H. *Angew. Chem., Int. Ed.* **2008**, *47*, 9618.
(28) Vareiro, M. M. L. M.; Liu, J.; Knoll, W.; Zak, K.; Williams, D.; Jenkins, A. T. A. *Anal. Chem.* **2005**, *77*, 2426.
(29) Velden, J. V.; Narolska, N. A.; Lamberts, R. R.; Boontje, N. M.; Borbely, A.; Zaremba, R.; Bronzwaer, J. G.; Papp, Z.; Jaquet, K.; Paulus, W. J.; Stienen, G. J. *Cardiovasc. Res.* **2006**, *69*, 876.
(30) Deligianni, D.; Katsala, N.; Ladas, S.; Sotiropoulou, D.; Amedee, J.; Missirlis, Y. *Biomaterials* **2001**, *22*, 1241.
(31) Wen, J. M.; Ruys, A. J.; Mason, R. S.; Martin, P. J.; Bendavid, A.; Liu, Z.; Ionescu, M.; Zreiqat, H. *Biomaterials* **2007**, *28*, 1620.
(32) Li, J.; Koehne, J. E.; Cassell, A. M.; Chen, H.; Ng, H. T.; Ye, Q.; Fan, W.; Han, J.; Meyyappan, M. *Electroanalysis* **2005**, *17*, 15.
(33) Advincula, M.; Fan, X.; Lemons, J.; Advincula, R. *Biointerfaces* **2005**, *42*, 29.
(34) Ban, N.; Escobar, C.; Carcia, R.; Hasel, K.; Day, J.; Greenwood, A. *Proc. Natl. Acad. Sci. U.S.A.* **1994**, *91*, 1604.
(35) Pease, L. F.; Elliott, J. T.; Tsai, D.; Zachariah, M. R.; Tarlov, M. J. *Biotechnol. Bioeng.* **2008**, *101*, 1214.